THE JOURNAL OF BIOLOGICAL CHEMISTRY VOL. 290, NO. 15, pp. 9377–9386, April 10, 2015

5-Azacytidine-induced Protein 2 (AZI2) Regulates Bone Mass by Fine-tuning Osteoclast Survival*

Received for publication, December 10, 2014, and in revised form, February 14, 2015 Published, JBC Papers in Press, February 17, 2015, DOI 10.1074/jbc.M114.631374

Kenta Maruyama[‡1], Masahiro Fukasaka[‡§], Satoshi Uematsu[¶], Osamu Takeuchi[‖], Takeshi Kondo[‡], Tatsuya Saitoh[‡], Mikaël M. Martino[‡], and Shizuo Akira[‡**2]**

*From the [‡]Laboratory of Host Defense, World Premier International (WPI) Immunology Frontier Research Center (IFReC), Osaka University, Osaka 565-0871, the [¶]Division of Innate Immune Regulation, International Research and Development Center for Mucosal Vaccine, Institute for Medical Science, The University of Tokyo, 4-6-1 Shirokanedai, Minato-ku, Tokyo 108-8639, the **Research Institute for Microbial Diseases, Osaka University, Osaka 565-0871, the [§]Life Science Research Center, Corporate R&D Development Division, Nitto Denko Corporation, 1-1-2 Shimohozumi, Ibaraki, Osaka 567-8680, and the [‖]Laboratory of Infection and Prevention, Institute for Virus Research, Kyoto University, 53 Shogokuin Kawara-cho, Sakyo-ku, Kyoto 606-8507, Japan*

Background: 5-Azacytidine-induced protein 2 (AZI2) is critical in GM-CSF-induced dendritic cell differentiation.
Results: *AZI2* deficiency enhances osteoclast survival, leading to decreased bone mass *in vivo*.
Conclusion: AZI2 suppresses osteoclast survival by inhibiting c-Src activation.
Significance: This is the first study showing the osteoprotective function of AZI2.

5-Azacytidine-induced protein 2 (AZI2) is a TNF receptor (TNFR)-associated factor family member-associated NF-κB activator-binding kinase 1-binding protein that regulates the production of IFNs. A previous *in vitro* study showed that AZI2 is involved in dendritic cell differentiation. However, the roles of AZI2 in immunity and its pleiotropic functions are unknown *in vivo*. Here we report that *AZI2* knock-out mice exhibit normal dendritic cell differentiation *in vivo*. However, we found that adult *AZI2* knock-out mice have severe osteoporosis due to increased osteoclast longevity. We revealed that the higher longevity of *AZI2*-deficient osteoclasts is due to an augmented activation of proto-oncogene tyrosine-protein kinase Src (c-Src), which is a critical player in osteoclast survival. We found that AZI2 inhibits c-Src activity by regulating the activation of heat shock protein 90 (Hsp90), a chaperone involved in c-Src dephosphorylation. Furthermore, we demonstrated that AZI2 indirectly inhibits c-Src by interacting with the Hsp90 co-chaperone Cdc37. Strikingly, administration of a c-Src inhibitor markedly prevented bone loss in *AZI2* knock-out mice. Together, these findings indicate that AZI2 regulates bone mass by fine-tuning osteoclast survival.

Bone-degrading osteoclasts are large multinucleated cells of myeloid lineage origin (1). It has been established that osteoclast differentiation and activation are induced by receptor activator of NF-κB ligand (RANKL)[3] expressed on bone-forming osteoblasts. After binding of RANKL to its receptor activator of NF-κB, transcription factors such as nuclear factor of activated T-cells cytoplasmic 1 (NFATc1) (2, 3), Jun dimerization protein 2 (Jdp2) (4, 5), c-Fos (6), and NF-κB (7) are activated, and osteoclast-specific genes are induced. Once the differentiation process is completed, osteoclasts undergo apoptosis. Recently, it has been suggested that the longevity of osteoclasts controls bone destruction. For example, osteoblast-derived cytokines such as macrophage colony-stimulating factor (M-CSF) (8) and osteopontin (OPN) (9) promote osteoclast survival. After the stimulation of osteoclast precursors by such survival factors, proto-oncogene tyrosine-protein kinase Src (c-Src), a non-receptor tyrosine kinase is activated and induces resistance to apoptosis (10, 11). c-Src activation is orchestrated by interplay between several other proteins. A recent study suggests that heat shock protein 90 (Hsp90), a molecular chaperone required for the stability of target proteins, suppresses c-Src activation (12). Moreover, previous studies revealed that Cdc37, a co-chaperone of Hsp90, directly binds to Hsp90 to strengthen interactions between Hsp90 and its binding partners, leading to enhanced chaperone activity of Hsp90 (13). Importantly, Hsp90 inhibitors such as 17-AAG disrupt the Hsp90-c-Src association, leading to the bone-degrading activity of osteoclasts via activation of c-Src. Therefore, the Hsp90 mediated regulation of the c-Src pathway is thought to be a novel therapeutic target for bone destructive diseases (12).

* This work was supported by a research fellowship from the Japan Society for the Promotion of Science (JSPS) for the Promotion of Science for Young Scientists, JSPS KAKENHI for a grant-in-aid for challenging exploratory research, a grant from the Osaka University MEET project, a grant from the Astellas Foundation for Research on Metabolic Disorders, a grant from the Naito Foundation, a grant from the SENSHIN Medical Research Foundation, a grant from the Japan Intractable Disease Research Foundation, and a visionary research grant from Takeda Science Foundation (to K. M.).

[1] To whom correspondence may be addressed: Laboratory of Host Defense, WPI Immunology Frontier Research Center, Osaka University, 3-1 Yamada-oka, Suita, Osaka 565-0871, Japan. Tel.: 81-6-6879-8303; Fax: 81-6-6879-8305; E-mail: maruyama@biken.osaka-u.ac.jp.

[2] To whom correspondence may be addressed: Shizuo Akira, Laboratory of Host Defense, WPI Immunology Frontier Research Center, Osaka University, 3-1 Yamada-oka, Suita, Osaka 565-0871, Japan. Tel.: 81-6-6879-8303; Fax: 81-6-6879-8305; E-mail: sakira@biken.osaka-u.ac.jp.

[3] The abbreviations used are: RANKL, receptor activator of NF-κB ligand; MDM, M-CSF-derived macrophage; μCT, micro computed tomography; TRAP, tartrate-resistant acid phosphatase; ALP, alkaline phosphatase; OPN, osteopontin; 17-AAG, 17-*N*-allylamino-17-demethoxygeldanamycin; TRAF, TNF receptor-associated factor; TANK, TRAF family member-associated NF-κB activator; PAP, pulmonary alveolar proteinosis; BAL, bronchoalveolar lavage; OVA, ovalbumin; qPCR, quantitative real-time PCR.

Regulation of osteoclast formation is also modulated by innate immune cytokines, such as IFNs (14). Type-I IFNs such as IFN-β are induced by RANKL and inhibit osteoclast differentiation (15). Virus-induced type-I IFN production is mediated by TNF receptor (TNFR)-associated factor family member-associated NF-κB activator-binding kinase 1 (TBK1) and IFN regulatory factor 3 (IRF3). Among the TBK1-binding proteins, TNF receptor-associated factor (TRAF) family member-associated NF-κB activator (TANK), 5-azacytidine-induced protein 2 (AZI2), and TBK1-binding protein 1 (TBKBP1) have been implicated in the production of type-I IFNs (14). However, our previous knock-out study revealed that TANK is dispensable for the production of IFNs (16), but indispensable for the suppression of excessive osteoclast formation via the inhibition of TRAF6 activation (17). We also generated *AZI2*- and *TBKBP1*-deficient mice and revealed that both genes were dispensable for IFN production (18). However, to our surprise, *AZI2*-deficient bone marrow cells exhibited impaired GM-CSF-mediated dendritic cell differentiation *in vitro* (18). GM-CSF is involved in the survival, maturation, proliferation, and differentiation of myeloid cells including dendritic cells (19). GM-CSF is also important in alveolar protein clearance because GM-CSF neutralizing autoantibodies are involved in the pathogenesis of pulmonary alveolar proteinosis (PAP) (20). Bronchoalveolar lavage (BAL) from PAP patients and *GM-CSF*-deficient mice contains lipoproteinaceous material consisting of surfactant proteins, and alveolar macrophages in BALs exhibit a large foamy appearance (20, 21). Importantly, such macrophages are also severely deficient in ATP-binding cassette subfamily G member 1 (ABCG1), a group of transmembrane proteins that play pivotal roles in mediating the cellular efflux of lipids, and peroxisome proliferator-activated receptor (PPAR)γ, a critical regulator of lipid homeostasis (22). Furthermore, lung tissues from PAP patients and *GM-CSF*-deficient mice exhibited many periodic acid-Schiff-positive alveolar fillings, leading to respiratory distress (20, 21, 23).

Despite the importance of AZI2 in GM-CSF signaling *in vitro*, the roles of AZI2 in immunity, lung homeostasis, and their functions in bone metabolism remain to be studied *in vivo*. Here we explored the role of AZI2 in host defense and bone homeostasis. We report that AZI2 is dispensable for GM-CSF signaling *in vivo*, but we found that *AZI2*-deficient mice have severe osteoporosis due to enhanced osteoclast survival.

EXPERIMENTAL PROCEDURES

Mice—AZI2- and *TBKBP1*-deficient mice were generated as described previously (18) and maintained in specific pathogen-free conditions. All animal experiments were performed in accordance with the approval of the Animal Research Committee of the Research Institute for Microbial Diseases (Osaka University, Osaka, Japan).

Cells and Reagents—For BAL harvest, the thoracic cavity was opened. After cannulation of the trachea, BAL fluid was collected by injecting PBS. T cells, B cells, and dendritic cells were isolated from total splenocytes by anti-Thy-1.2, anti-B220, and anti-CD11c magnetic beads (Miltenyi Biotec, Bergisch Gladbach, Germany), respectively. Splenic $CD11b^+$ macrophages were sorted by a FACSAria (BD Biosciences). To generate Th cells, $CD4^+$ cells were isolated by anti-CD4 magnetic beads (Miltenyi Biotec) and used to generate Th1, Th2, or Th17 cells, as described previously (24). Synovial fibroblasts were prepared as described previously. (25) For $CD4^+$ T proliferation assays, splenic CD11c-positive cells were stimulated with 1 μg/ml LPS for 24 h and irradiated (3000 radians). Balb/c-derived splenic $CD4^+$ T cells were mixed with irradiated cells, and after 72 h, $CD4^+$ T proliferation was measured as described previously (18). LPS from *Salmonella minnesota* strain Re-595 was purchased from Sigma-Aldrich. Other reagents purchased included recombinant murine RANKL (462-TR, R&D Systems), murine M-CSF (315-02, PeproTech), murine OPN (441-OP-200, R&D Systems), c-Src inhibitor AZ0530 (1010-80, AdooQ Bioscience), ELISA kit for mouse cross-linked C-telopeptide of type-I collagen (USCN Life Science Inc.), RANKL ELISA kit (MTR00, R&D Systems), osteoprotegerin (OPG) ELISA kit (MOP00, R&D Systems), cell death detection ELISA (Roche Applied Science), ELISA kits for TNF, IL-6, and IL-12 (R&D Systems), and ALP quantification kit (LabAssay, Wako Chemicals, Tokyo, Japan). Nuclear extracts were prepared as described (16), and the DNA binding of NF-κB p65 and NFATc1 was quantified using a TransAM transcription factor assay (Active Motif, Carlsbad, CA). Antibodies for FACS analysis were purchased from BD Biosciences. Data were collected by FACSCalibur (BD Biosciences) and analyzed by FlowJo (Ashland, OR).

In Vivo Immunization—Mice were intraperitoneally immunized with 10 μg of ovalbumin (OVA) (Sigma) plus alum (LG6000 LSL, Cosmo Bio). Serum OVA-specific IgG1 and OVA-specific IgM were measured by mouse anti-OVA IgG1 EIA kit (500830, Cayman Chemical) and mouse anti-OVA IgM ELISA kit (600-170-OGM, Alpha diagnostic), respectively.

In Vivo Infection—Staphylococcus aureus was cultured in tryptic soy broth for 15 h at 37 °C. Mice were infected intravenously with a PBS solution containing 5×10^7 *S. aureus*.

Analysis of in Vivo Bone Phenotype—To check the bone formation rate, double calcein labeling was performed as described (26). For bone histomorphometric analysis, tibias were stained with Villanueva bone stain (Wako Chemicals) and embedded in methyl-methacrylate. Serial longitudinal sections (6-mm-thick) were generated, and each section was observed by a Histometry RT camera (System Supply Co., Ltd., Nagano, Japan). Distal portions of femurs were analyzed by three-dimensional microcomputed tomographic (μCT) using Scan-Xmate RB080SS110 (Comscan Techno Co., Ltd., Sagamihara, Japan) and TRI/3D-Bon software (Ratoc System Engineering Co., Ltd., Tokyo, Japan). Bone microarchitectural parameters were quantified in the trabecular regions at 0.1–1.5 mm from the chondro-osseous junction.

Immunoblotting and Immunoprecipitation—Western blotting was performed as described previously (16). Proteins were detected using anti-phospho-Src (2101, Cell Signaling) and anti-actin (C-11, Santa Cruz Biotechnology Inc.) antibodies. For immunoprecipitation, cell lysates were incubated with protein A-Sepharose (GE Healthcare) containing 3 μg of anti-Cdc37 antibodies (E-4; Santa Cruz Biotechnology), anti-AZI2 antibodies (ab65242, Abcam), anti-Hsp90 antibodies (3389-100, Bio Vision), or control IgG for 1 h at 4 °C. The immunoprecipitants were washed, eluted, and then analyzed by West-

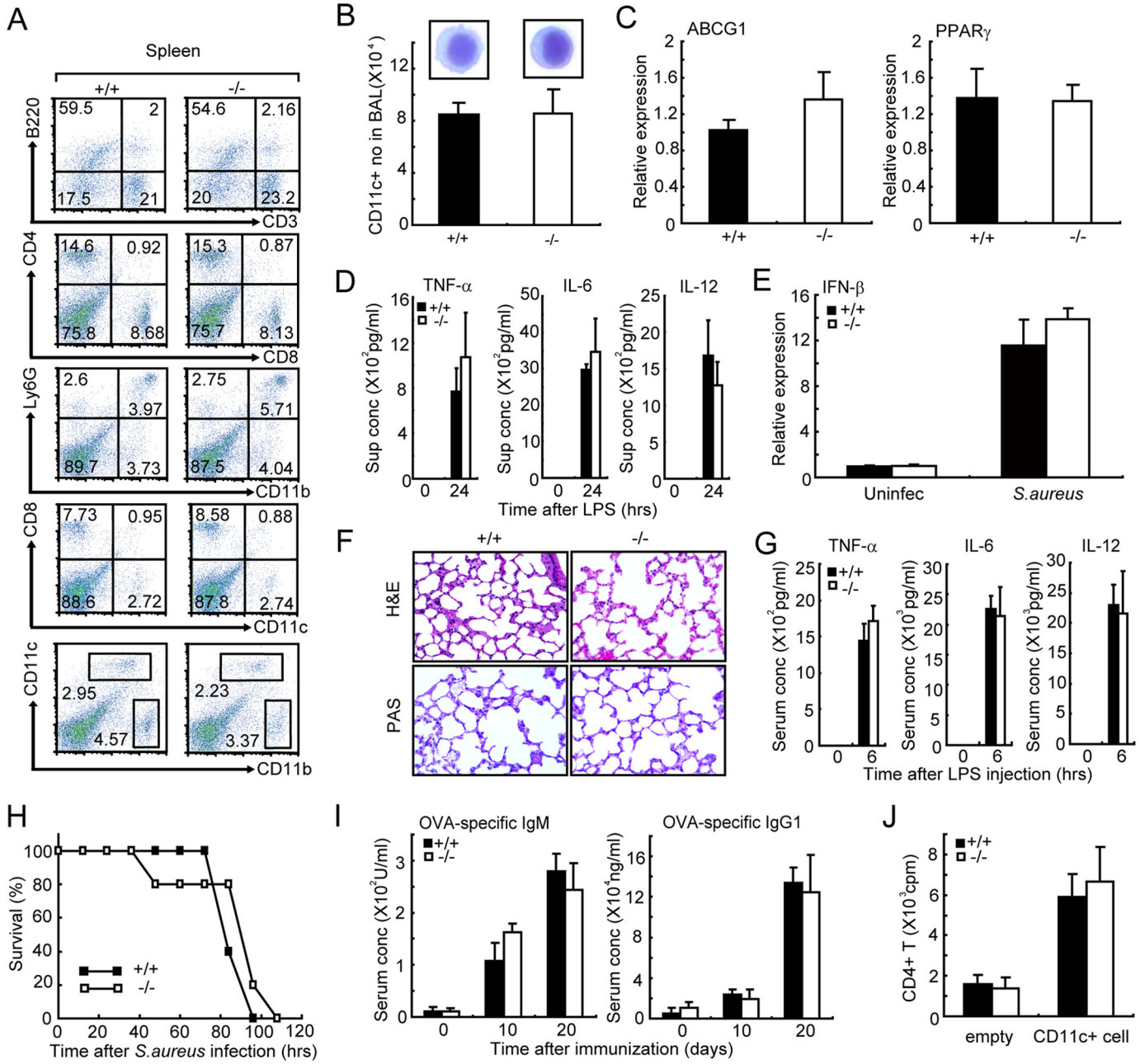

FIGURE 1. **AZI2 is dispensable for *in vivo* myeloid cell differentiation and function.** *A*, splenic cells were stained with the indicated antibodies and analyzed by FACS. *B*, $CD11c^+$ cell numbers from BAL of *AZI2*-deficient mice. Representative pictures of $CD11c^+$ cells are shown. *C*, expression of ABCG1 and PPARγ in $CD11c^+$ cell from BAL. *D*, $CD11c^+$ cells in *B* were sorted and stimulated with LPS for 24 h. Cytokine production was measured by ELISA. *Sup conc*, supernatant concentration. *E*, mice were intravenously infected with *S. aureus*. After 24 h, BAL cells were harvested, and IFN-β mRNA levels were measured by qPCR. *F*, representative histological images of lung (*upper*: H&E staining; *lower*: periodic acid-Schiff (*PAS*) staining). *G*, serum cytokine concentrations (*Serum conc*) after intraperitoneal injection of 1 mg/ml LPS. *H*, *S. aureus* was intravenously injected into mice, and survival was monitored for the indicated times ($n = 5$). *I*, Mice were immunized with OVA plus alum. Serum levels of OVA-specific IgM and OVA-specific IgG1 were measured by ELISA. *J*, splenic $CD11c^+$ cells were stimulated with LPS for 24 h and irradiated. $CD4^+$ T cells from Balb/c mice were added to the culture, and proliferation of T cells was quantified by [^{3}H]thymidine incorporation. *Error bars*, S.E. $n = 3$, unless indicated.

ern blotting as described previously (16). Immunoprecipitated proteins were detected using ImmunoCruz IP/WB Optima system (Santa Cruz Biotechnology) antibodies. To detect activation of caspase-3, anti-cleaved caspase-3 antibody (Cell Signaling) was purchased.

Osteoclast and Osteoblast Culture—M-CSF-derived macrophages (MDMs) were prepared as described (27) and used as osteoclast precursors. Osteoclast differentiation was induced in the presence of 25 ng/ml M-CSF for various times and with various concentrations of RANKL. TRAP staining was performed as described (17). For the osteoclast survival assay, MDMs were cultured with RANKL for 84 h. Then, RANKL and M-CSF were removed, and osteoclasts were cultured for an additional 36 h. The survival rate was quantified by counting morphologically intact osteoclasts. For the osteoclast/osteoblast co-culture assay, calvarial cells (5×10^5) and MDMs (3×10^5) were cultured in the presence of prostaglandin E_2 (PGE_2) and 1α,25-dihydroxyvitamin D_3 ($1\alpha,25(OH)_2D_3$). For analysis

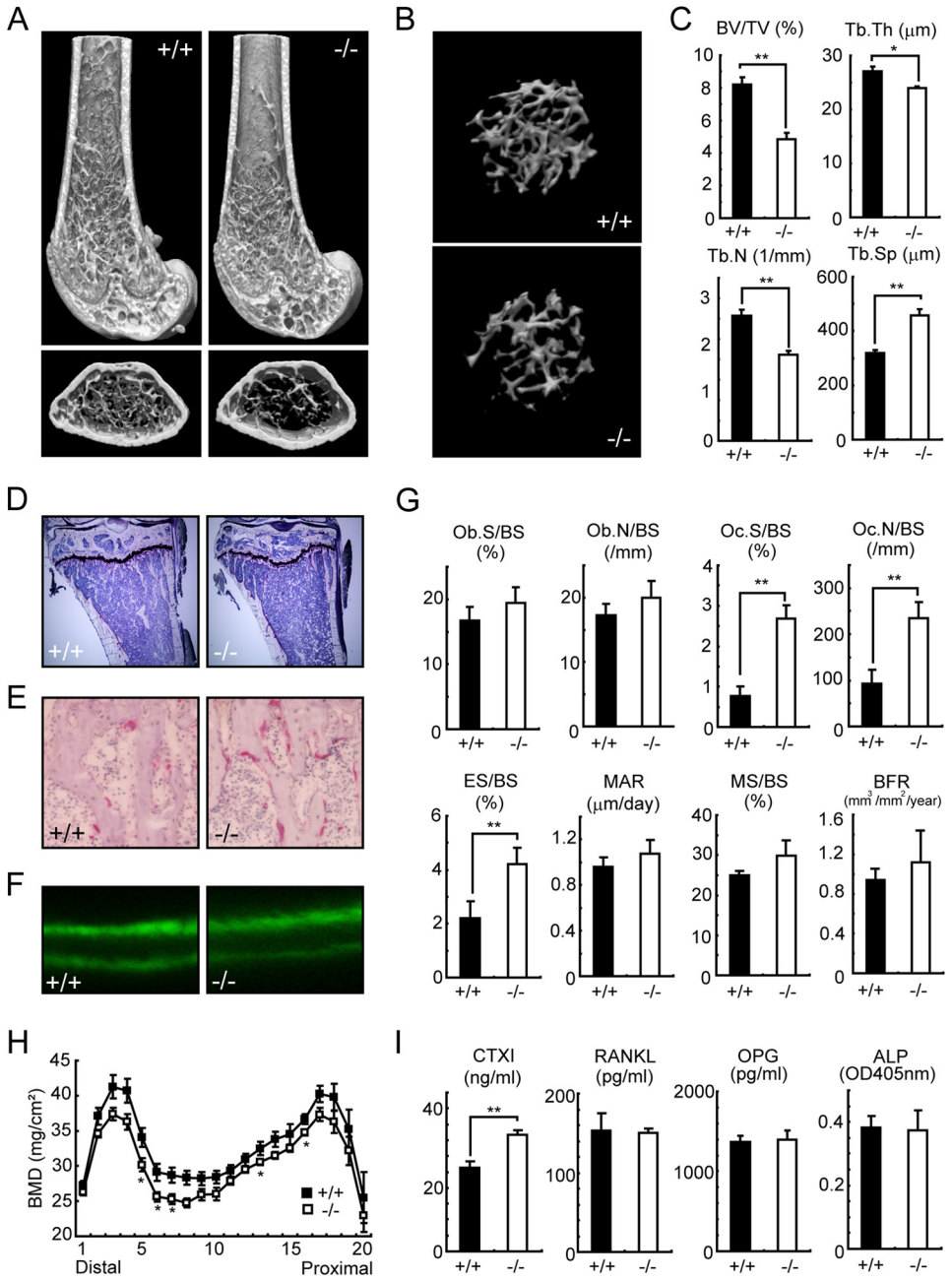

FIGURE 2. ***AZI2*-deficient mice (10-week-old female mice) are osteoporotic.** *A*, representative μCT images of distal femurs from longitudinal view (*upper*) and from axial view (*lower*). *B*, representative three-dimensional μCT view of metaphyseal portion of femur. *C*, bone morphometric analysis of distal femurs by μCT. *Error bars*, S.E. *, $p < 0.05$, **, $p < 0.01$ ($n = 5$). *BV/TV*, bone volume per tissue volume; *Tb.Th*, trabecular bone thickness; *Tb.N*, trabecular bone number; *Tb.Sp*, trabecular bone spacing. *D*, representative images of proximal portion of tibias. *E*, representative images of osteoclasts in the proximal portion of tibias (TRAP staining). *F*, representative images of double calcein staining. *G*, bone histomorphometric analysis of the metaphyseal portion of tibias. *Error bars*, S.E. **, $p < 0.01$ ($n = 4$–5). *Ob.S/BS*, osteoblast surface per bone surface; *Ob.N/BS*, osteoblast number per bone surface; *Oc.S/BS*, osteoclast surface per bone surface; *Oc.N/BS*, osteoclast number per bone surface; *ES/BS*, eroded surface per bone surface; *MAR*, mineral apposition rate; *MS/BS*, mineralized surface per bone surface; *BFR*, bone formation rate. *H*, bone mineral densities (*BMD*) of femurs. S.E. *, $p < 0.05$, ($n = 4$). *I*, serum levels of bone metabolism markers. S.E. **, $p < 0.01$ ($n = 4$). *CTXI*, C-terminal telopeptides type I collagen; *OPG*, osteoprotegerin; *OD*, optical density.

of osteoclast resorptive activity, MDMs were plated on bone resorption assay plates (Iwai Chemical Co., Tokyo, Japan). After 5 days of RANKL stimulation, plates were immersed in 1 M NH_4OH, and pit numbers were counted. Calvariae from newborn mice were digested in α-MEM containing 0.1% collagenase and 0.2% dispase at 37 °C for 20 min. Mesenchymal stem cells from compact bone were prepared as described (28). To generate osteoblasts *in vitro*, calvarial cells or mesenchymal stem cells were cultured in an osteoblast inducer reagent (Takara). ALP and calcified nodules in osteoblast cultures were detected using a TRAP/ALP staining kit (Wako Chemicals) and calcified nodule staining kit (AK-21; Primary Cell Co., Ltd., Hokkaido, Japan), respectively. Calcium concentrations were measured using a kit (Metalloassay LS-MPR, AKJ Global Technology).

Calcium Imaging—Cells were plated on poly-L-lysine-coated glass-bottom dishes and cultured with Fura2/AM. Fluorescent activities were analyzed as described previously (29).

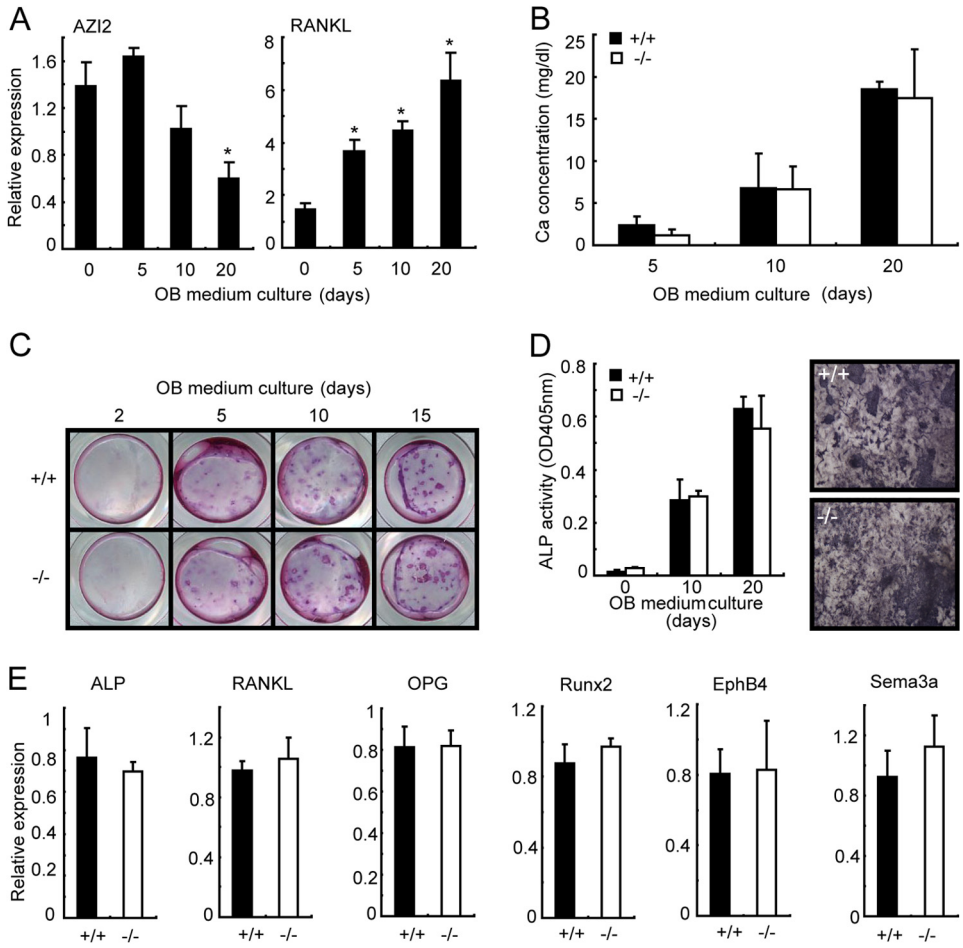

FIGURE 3. **Osteoblastogenesis is normal in *AZI2*-deficient cells.** *A* and *B*, calvariae were cultured in osteoblast (*OB*)-inducing medium, and AZI2 expression levels (*A*) or calcium concentrations (*B*) were measured. *C*, representative images of calcified nodules. *D*, calvariae were cultured with osteoblast-inducing medium, and ALP activities were measured. Representative ALP staining pictures at day 10 are shown in the *right panels*. *OD*, optical density. *E*, qPCR analysis of osteoblast differentiation markers from cells in *C*. *Error bars*, S.E. *, $p < 0.05$, ($n = 3$). *OPG*, osteoprotegerin.

PCR—RNA was extracted using TRIzol reagent (Life Technologies) and reverse-transcribed by ReverTra Ace (Toyobo Co., Ltd., Osaka, Japan). Quantitative real-time PCR (qPCR) was performed using an ABI PRISM 7500 real time PCR system. TaqMan Assays-on-Demand primers were purchased from Applied Biosystems (Foster City, CA).

Viral Gene Transfer/Knockdown—AZI2 was cloned into a retroviral vector and transfected into the packaging cell line PlatE. Retroviral gene transduction of MDMs was performed as described previously (30). After transduction, cells were stimulated with RANKL. Cdc37 shRNA lentiviral particles (sc-35043-V) and control particles (sc-108080) were purchased from Santa Cruz Biotechnology. For lentiviral gene transfer, virus was added to wells with Polybrene. After 20 h, cells were stimulated with RANKL to induce osteoclasts.

Statistical Analysis—Student's *t* test was used to evaluate statistical significance, with significance set at $p < 0.05$.

RESULTS

AZI2 Is Dispensable for in Vivo Myeloid Cell Differentiation and Function—Because AZI2 is critical for *in vitro* GM-CSF signaling, we hypothesized that *AZI2*-deficient mice would exhibit PAP. We first evaluated the population of myeloid and lymphoid cell lineages in *AZI2*-deficient mice, but hematopoiesis was normal (Fig. 1*A*). Unexpectedly, the number of alveolar macrophages in *AZI2*-deficient mice was normal. Moreover, alveolar macrophages presented normal morphology, cytokine production, and lipid metabolism-associated gene expression (Fig. 1, *B–E*). Furthermore, alveolar structures of *AZI2*-deficient mice were normal, and periodic acid-Schiff-positive alveolar fillings were not detected in these mice (Fig. 1*F*). Because GM-CSF-induced *AZI2*-deficient dendritic cells have shown impaired Toll-like receptor (TLR) signaling and antigen-presenting activity (18), we evaluated the production of cytokine and acquired immune functions in *AZI2*-deficient mice. However, *AZI2* deficiency had no impact on the production of proinflammatory cytokines or survival in response to LPS (Fig. 1*G*), *S. aureus* (Fig. 1*H*), and *Candida albicans* (data not shown). Additionally, the production of OVA-specific IgM and IgG1 in response to intraperitoneal injection of OVA plus alum was normal in *AZI2*-deficient mice (Fig. 1*I*). Furthermore, *AZI2* deficiency had no impact on T cell activation by CD11c-positive splenocytes (Fig. 1*J*). Thus, these findings indicate that TBK1-binding protein AZI2 is dispensable for myeloid cell differentiation and functions *in vivo*.

AZI2-deficient Mice Are Osteoporotic—During the flushing of bone marrow from 11-week-old mice, we noticed that *AZI2*-

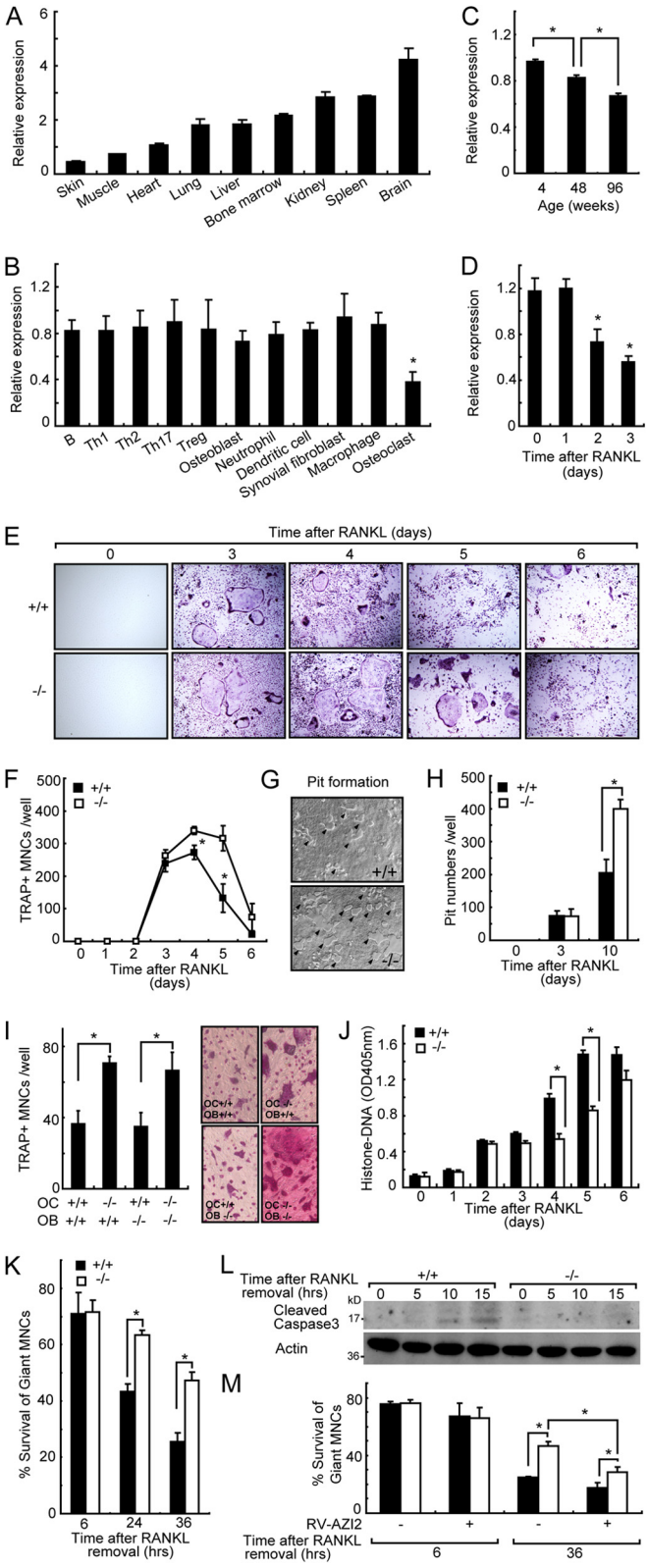

FIGURE 4. **Increased survival of *AZI2*-deficient osteoclasts.** *A* and *B*, indicated organs (*A*) and cells (*B*) were collected, and AZI2 expression levels were analyzed by qPCR. *C*, bone marrow cells from variously aged mice were harvested, and osteoclastogenesis was induced by RANKL stimulation. Expression of AZI2 was measured by qPCR. *D*, AZI2 expression levels during RANKL-induced osteoclastogenesis were quantified by qPCR. *E*, MDMs were cultured in the presence of 75 ng/ml RANKL for the indicated times. Representative TRAP staining is shown. *F*, TRAP-positive cell numbers in *E* were counted. *MNCs*, multinucleated cells. *G* and *H*, MDMs were cultured on dentine slice resorption pits and analyzed under a microscope (*G*), and pit numbers were counted (*H*). *I*, bone marrow cells and calvariae were co-cultured, and TRAP-positive cell numbers were counted. Representative images are shown (*right*). *J*, MDMs were cultured in the presence of 75 ng/ml RANKL. Histone-DNA levels in culture supernatants were quantified by ELISA. *OD*, optical density. *K*, osteoclast survival assay was performed. *Giant MNCs* = >10 nuclei/TRAP-positive multinucleated cells. *L*, cleaved caspase-3 levels in osteoclast survival assay were measured by Western blotting. *M*, osteoclast survival assay was performed after infection of retrovirus encoding AZI2 (RV-AZI2). *Error bars*, S.E. *, $p < 0.05$, ($n = 4$).

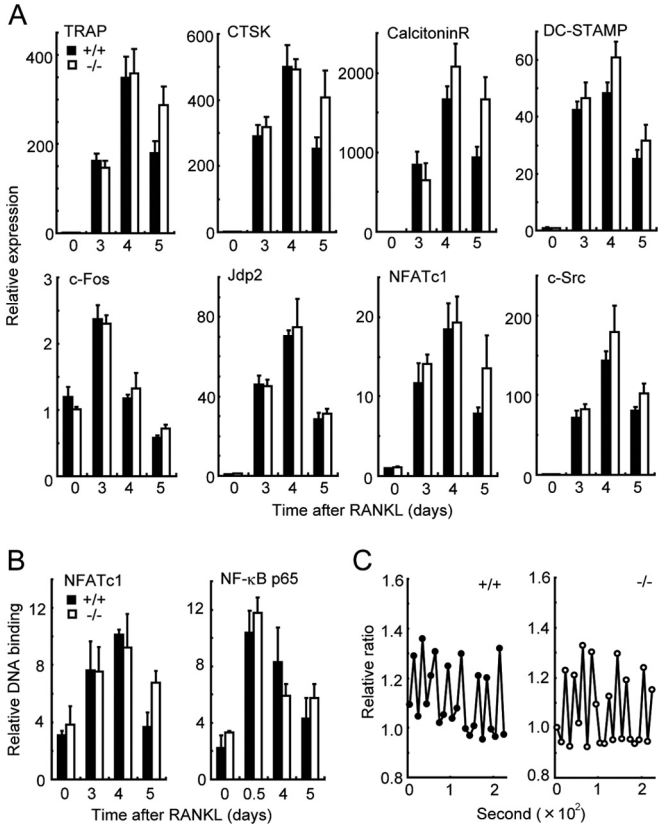

FIGURE 5. **Differentiation is normal in *AZI2*-deficient osteoclasts.** *A*, MDMs were cultured in the presence of 75 ng/ml RANKL. Cells were harvested for the indicated times, and osteoclast differentiation markers were measured by qPCR. *Error bars*, S.E., ($n = 3$). *CTSK*, cathepsin K; *CalcitoninR*, calcitonin receptor; *DC-STAMP*, dendritic cell-specific transmembrane protein. *B*, MDMs were treated with 175 ng/ml RANKL. Nuclear extracts were harvested, and DNA binding activity of NFATc1 and NF-κB was measured. *Error bars*, S.E., ($n = 3$). *C*, MDMs were treated with 100 ng/ml RANKL for 24 h, and calcium imaging was performed. Representative traces of fura-2 fluorescence ratios are shown.

deficient femurs were more fragile when compared with wild-type control mice. Thus, this observation prompted us to explore the role of AZI2 in bone homeostasis. Body weight and femur length were normal in *AZI2*-deficient mice, but μCT analysis of the distal portion of femurs revealed dramatically impaired trabecular bone volume and number when compared with wild-type mice (Fig. 2, *A*–C). Bone histomorphometric analysis of proximal tibias from *AZI2*-deficient mice showed a significant reduction of the trabecular bone area accompanied by a dramatic increase of osteoclast number and eroded area (Fig. 2, *D*–*G*). In contrast, osteoblast parameters and bone-forming rate were normal (Fig. 2, *F* and *G*). Consistent with the high number of osteoclasts, the bone mineral density in cortical

areas of femurs was significantly decreased and the serum bone resorption marker C-terminal telopeptides type I collagen (CTXI) was increased in *AZI2*-deficient mice (Fig. 2, *H* and *I*). Thus, these data clearly indicate that *AZI2*-deficient mice are osteoporotic. In contrast, femurs and osteoclasts from *TBKBP1*-deficient mice were normal (data not shown).

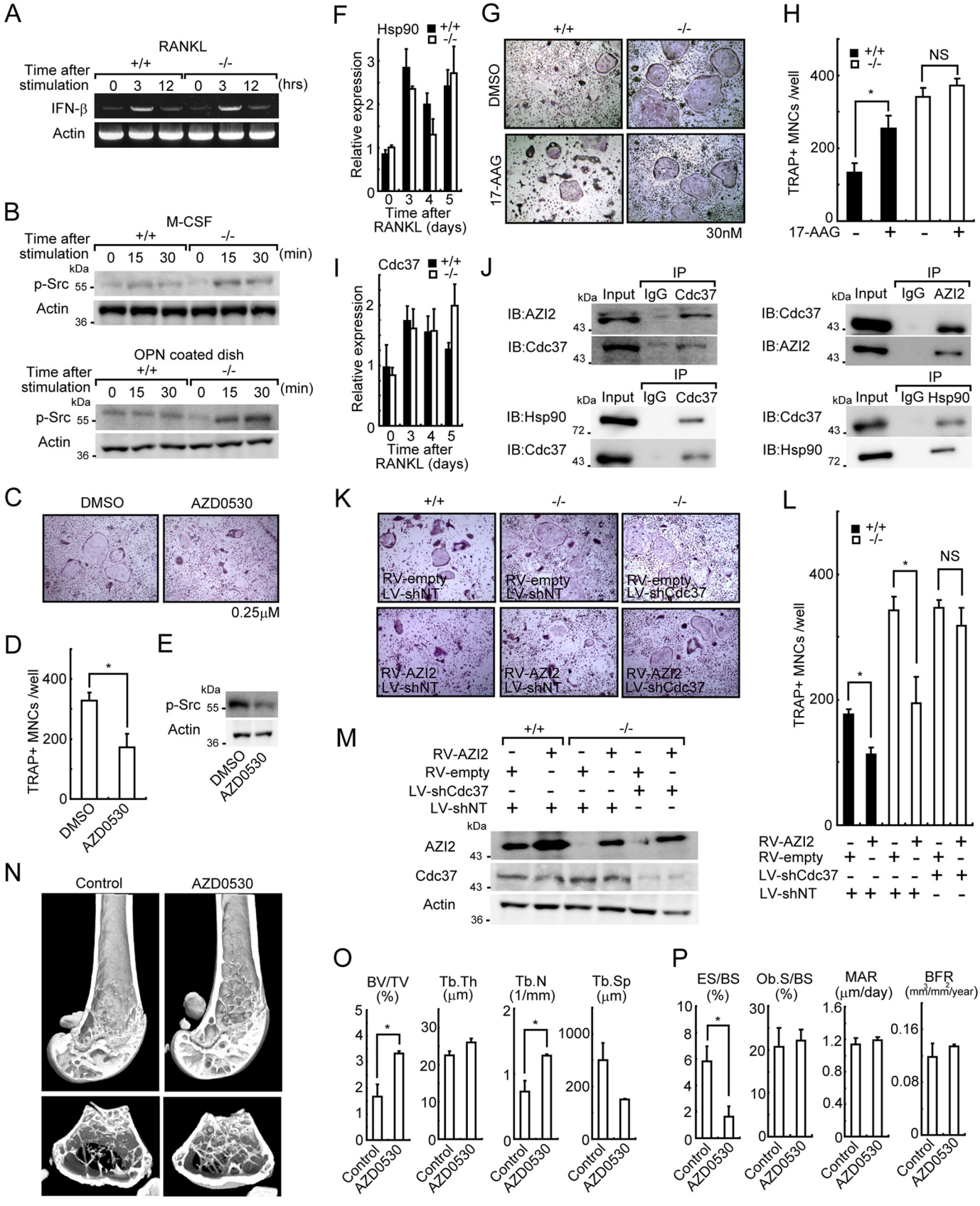

Osteoblast Functions Are Normal in AZI2 Deficiency—Because the osteoporotic phenotype of *AZI2*-deficient mice could be due to impaired osteoblast functions, we explored the role of AZI2 in osteoblasts. First, we found that the expression level of AZI2 in osteoblasts considerably decreases during differentiation (Fig. 3*A*). Next, we cultured calvarial cells with osteoblast-inducing medium and analyzed their calcification potential. However, *AZI2* deficiency did not affect bone nodule formation (Fig. 3, *B* and *C*). Furthermore, the expression levels of osteoblast differentiation markers such as ALP, RANKL, OPG, and Runx2 were normal (Fig. 3, *D* and *E*). Recently, it has been reported that osteoblast-derived factors such as EphB4 and Sema3a are involved in osteoclast suppression. Because these osteoblast-osteoclast communicating factors are critical for bone remodeling, we further checked the expression of these genes, but *AZI2* deficiency had no impact on gene expression (Fig. 3*E*). Collectively, these findings suggest that AZI2 does not affect osteoblast differentiation and function both *in vitro* and *in vivo*.

Increased Survival of AZI2-deficient Osteoclasts—AZI2 is broadly expressed in various organs, especially bone marrow, kidney, spleen, and brain (Fig. 4*A*). This suggests that AZI2 is predominantly expressed in hematopoietic and neural systems. We also analyzed the AZI2 expression levels in various cells and found that AZI2 expression is lower in osteoclasts when compared with lymphocytes, myeloid cells, osteoblasts, and synovial cells (Fig. 4*B*). Importantly, osteoclasts from old mice exhibited significantly lower expression of AZI2 when compared with young mice, and the expression level of AZI2 in MDMs gradually decreased during RANKL-induced osteoclastogenesis (Fig. 4, *C* and *D*). To explore the role of AZI2 during osteoclastogenesis, we analyzed the differentiation of *AZI2* knock-out mouse-derived MDMs into osteoclasts. Three days after RANKL-induced osteoclastogenesis, the number of osteoclasts generated was comparable between *AZI2*-deficient MDMs and wild-type MDMs (Fig. 4, *E* and *F*). However, 5 days after RANKL stimulation, wild-type cells began to die and the number of TRAP-positive multinucleated cell was lower when compared with day 4 (Fig. 4, *E* and *F*). In contrast, *AZI2*-deficient cells exhibited a high number of TRAP-positive multinucleated cells, even at day 5 (Fig. 4, *E* and *F*). Confirming the improved osteoclast activity of *AZI2*-deficient osteoclasts, the number of bone resorption pits generated by *AZI2*-deficient osteoclasts was significantly higher when compared with wild-type osteoclasts. However, this improvement of osteoclast activity was not due to an enhanced osteoblast-supporting function (Fig. 4, *G–I*). Importantly, osteoclast survival assay showed that *AZI2*-deficient osteoclasts have a significantly slower apoptosis (Fig. 4, *J* and *K*). Confirming this slower apoptosis rate, *AZI2*-deficient osteoclasts have a lower concentration of cleaved caspase-3, which is a critical executioner of apoptosis (Fig. 4*L*). Furthermore, slower apoptosis level in *AZI2*-deficient osteoclasts was partially rescued by AZI2 expression (Fig. 4*M*). Nevertheless, the expression levels of osteoclastic genes (Fig. 5*A*), calcium oscillation, and activation of osteoclast-inducing transcription factors such as NFATc1 and NF-κB (Fig. 5, *B* and *C*) were similar in both *AZI2*-deficient osteoclasts and wild-type osteoclasts. Together, these observations clearly show that *AZI2*-deficient osteoclasts are defective for apoptosis pathways, but exhibit normal differentiation.

AZI2 Regulates c-Src Activation—To gain insight into the mechanism underlying the aberrant osteoclastogenesis in *AZI2*-deficient mice, we analyzed RANKL and M-CSF signaling. First, because AZI2 is implicated in the production of IFN-β, and because RANKL can also induce IFN-β, we quantified the expression of IFN-β induced by RANKL in *AZI2*-deficient MDMs (Fig. 6*A*). However, *AZI2*-deficient MDMs exhibited normal IFN-β expression in response to RANKL (Fig. 6*A*). Next, because M-CSF and OPN promote osteoclast survival via activation of c-Src, we stimulated *AZI2*-deficient osteoclasts with M-CSF or OPN and measured the level of phosphorylated c-Src level (Tyr(P)-416 Src) by Western blotting (Fig. 6*B*). Intriguingly, the activation of c-Src was enhanced in *AZI2*-deficient cells, in response to M-CSF or OPN stimulation (Fig. 6*B*), and a c-Src inhibitor AZD0530 suppressed excessive osteoclast generation in *AZI2*-deficient cells (Fig. 6, *C–E*). To clarify the molecular mechanisms leading to an enhanced c-Src activation in *AZI2*-deficient cells, we measured the expression levels of Hsp90, which is a potent inhibitor of c-Src activation (Fig. 6*F*). Unexpectedly, Hsp90 expression in *AZI2*-deficient osteoclasts was normal (Fig. 6*F*). Notably, a Hsp90 inhibitor, 17-AAG, significantly increased osteoclast numbers in wild-type cells, but *AZI2*-deficient cells did not respond to this inhibitor (Fig. 6, *G* and *H*). Moreover, the expression levels of Cdc37, which is a critical binding partner of Hsp90 for the inhibition of c-Src, were comparable between wild-type and *AZI2* knock-out cells (Fig. 6*I*). Because the Hsp90 inhibitor had no effect on osteoclast formation in *AZI2*-deficient cells, we predicted that AZI2 may be a component of the functional Hsp90-Cdc37 complex. To confirm this hypothesis, we examined the associ-

FIGURE 6. **Enhanced c-Src activation in *AZI2*-deficient osteoclasts.** *A*, MDMs were stimulated with 300 ng/ml RANKL for the indicated times. IFN-β expression levels were measured by PCR. *B*, MDMs were cultured with 75 ng/ml RANKL for 60 h and then starved for 6 h, removed, and stimulated with 300 ng/ml M-CSF medium or replated on OPN (20 μg/ml)-coated dishes. Cells were harvested at the indicated times, and phospho-Src (*p-Src*) levels were quantified by Western blotting. *C–E*, *AZI2*-deficient MDMs were treated with 75 ng/ml RANKL plus Src inhibitor AZD0530 (0.25 μM) for 4 days. Representative TRAP staining (*C*), p-Src protein levels (*D*), and TRAP-positive cell numbers (*E*) are shown. *DMSO*, dimethyl sulfoxide; *MNCs*, multinucleated cells. *F*, MDMs were stimulated with 75 ng/ml RANKL, and Hsp90 levels measured by qPCR. *G* and *H*, MDMs were treated with 75 ng/ml RANKL plus Hsp90 inhibitor 17-AAG (30 nM) for 4.5 days. Representative TRAP staining (*G*) and TRAP-positive cell numbers (*H*) are shown. *NS*, not significant. *I*, MDMs were stimulated with 75 ng/ml RANKL, and Cdc37 levels were measured by qPCR. *J*, immunoprecipitation (*IP*) of wild-type MDM lysates. After anti-Cdc37, anti-AZI2, and anti-Hsp90 immunoprecipitation, precipitates were analyzed by Western blotting (*IB*) using the indicated antibodies. *K*, representative TRAP staining of osteoclasts after infection of retrovirus encoding AZI2 (*RV-AZI2*), empty retrovirus (*RV-empty*), lentivirus encoding shCdc37 (*LV-shCdc37*), and lentivirus encoding nontargeting shRNA (*LV-shNT*). *L*, TRAP-positive cell numbers. *M*, expression levels of AZI2 and Cdc37 were measured by Western blotting. *N–P*, 9-week-old *AZI2*-deficient mice were orally inoculated with AZD0530 (50 mg/kg, 4 times/week). After 5 weeks, bones were analyzed by μCT. Representative μCT images of distal femurs (*N*), bone morphometric analysis of distal femurs (*O*), and bone histomorphometric analysis of the metaphyseal portion of tibias (*P*) are shown. *BV/TV*, bone volume per tissue volume; *Tb.Th*, trabecular bone thickness; *Tb.N*, trabecular bone number; *Tb.Sp*, trabecular bone spacing; *ES/BS*, eroded surface/bone surface; *Ob.S/BS*, osteoblast surface/bone surface; *MAR*, mineral apposition rate; *BFR*, bone-forming rate. *Error bars*, S.E. *, $p < 0.05$, ($n = 3$).

ation of AZI2 with Cdc37. As expected, an association between Hsp90 and Cdc37 was observed by immunoprecipitation of mouse primary MDMs (Fig. 6*J*). Intriguingly, an association between AZI2 and Cdc37 was also identified (Fig. 6*J*). Furthermore, retroviral expression of AZI2 significantly rescued excessive osteoclast formation in *AZI2*-deficient cells, but not in Cdc37 knockdown *AZI2*-deficient cells (Fig. 6, *K–M*). Thus, these findings clearly indicate that the Hsp90-Cdc37-AZI2 complex is critical for the suppression of c-Src activation in osteoclasts. Finally, oral administration of a c-Src inhibitor, AZD0530, significantly rescued the osteoporotic phenotype of *AZI2*-deficient mice (Fig. 6, *N–P*). Based on these data, we concluded that AZI2 regulates bone mass by fine-tuning c-Src activation in osteoclasts.

DISCUSSION

Previous studies demonstrated that among the TBK1-binding proteins, TANK, AZI2, and TBKBP1 regulated the production of type-I IFNs *in vitro* (14). In contrast, our knock-out mouse studies revealed that TANK, AZI2, and TBKBP1 are dispensable for IFN production *in vivo*. In addition, we have demonstrated that AZI2 is indispensable for *in vitro* GM-CSF-induced dendritic cell differentiation (18), and it has been reported that GM-CSF signaling is critical for alveolar protein clearance by macrophages (20, 21). Here, to our surprise, we could not observe any immunological or alveolar abnormalities in *AZI2*-deficient mice. Although GM-CSF is predominantly used as an inducer of dendritic cells *in vitro*, *GM-CSF*-deficient mice exhibit normal dendritic cell populations (20, 21). Thus, we speculate that *in vivo* GM-CSF signaling is dispensable for dendritic cell differentiation, but indispensable for proper functions of lung macrophages. Most likely, additional studies are needed to clarify the molecular functions of AZI2 in dendritic cells, but our data clearly indicate that the *in vitro* signaling defects of GM-CSF in *AZI2*-deficient cells are compensated by unknown mechanisms *in vivo*.

Although we did not detect any immunological or alveolar abnormalities in *AZI2*-deficient mice, we discovered that they are osteoporotic. We found that c-Src activation is enhanced in *AZI2*-deficient osteoclasts, when they are stimulated by osteoclast survival factors such as M-CSF or OPN. Recently, it was reported that disruption of Hsp90-c-Src binding by 17-AAG stimulates c-Src activation (12), and previous studies also suggested that Cdc37 is critical for the Hsp90 inhibitory function on c-Src (13). Here, we demonstrate that AZI2 regulates the c-Src repressive activity of Hsp90 by directly binding to Cdc37. Moreover, because the expression of AZI2 gradually decreases during osteoclast differentiation, whereas the expression of Hsp90 and Cdc37 increases during this process, AZI2 expression levels might regulate the c-Src repressive activity of the Hsp90-Cdc37 complex.

In our previous knock-out study, we found that TANK negatively regulates osteoclast formation by suppressing the activation of TRAF6 (16). In this study, we show that AZI2, but not TBKBP1, also functions as a negative regulator of osteoclast formation by suppressing the activity c-Src. Therefore, we suggest that these TBK1-binding partner proteins are indispensable for proper bone homeostasis.

Although further experiments are required to understand the precise molecular mechanisms of AZI2 in osteoclastogenesis, our data clearly indicate that AZI2 plays a pivotal role by fine-tuning osteoclast survival. Moreover, our findings provide a basis for AZI2-stimulating therapeutic strategies to treat osteoporosis and rheumatoid arthritis.

Acknowledgments—We thank E. Kamada for secretarial assistance, and Y. Fujiwara and M. Kumagai for technical assistance.

Note Added in Proof—The Abstract and Discussion contain two errors in the version of this article that was published on February 17, 2015 as a Paper in Press, which misrepresent the interpretation of the results. These errors have been corrected by replacing "We found that AZI2 promotes c-Src activity, by inhibiting the heat shock protein 90 (Hsp90)-a chaperone involved in c-Src dephosphorylation." in the Abstract with "We found that AZI2 inhibits c-Src activity, by regulating the activation of heat shock protein 90 (Hsp90), a chaperone involved in c-Src dephosphorylation." and by replacing "Here, we demonstrate that AZI2 inhibits the c-Src repressive activity of Hsp90, by directly binding to Cdc37." with "Here, we demonstrate that AZI2 regulates the c-Src repressive activity of Hsp90, by directly binding to Cdc37." in the Discussion.

REFERENCES

1. Karsenty, G., and Wagner, E. F. (2002) Reaching a genetic and molecular understanding of skeletal development. *Dev. Cell* **2,** 389–406
2. Takayanagi, H., Kim, S., Koga, T., Nishina, H., Isshiki, M., Yoshida, H., Saiura, A., Isobe, M., Yokochi, T., Inoue, J., Wagner, E. F., Mak, T. W., Kodama, T., and Taniguchi, T. (2002) Induction and activation of the transcription factor NFATc1 (NFAT2) integrate RANKL signaling in terminal differentiation of osteoclasts. *Dev. Cell* **3,** 889–901
3. Matsuo, K., Galson, D. L., Zhao, C., Peng, L., Laplace, C., Wang, K. Z., Bachler, M. A., Amano, H., Aburatani, H., Ishikawa, H., and Wagner, E. F. (2004) Nuclear factor of activated T-cells (NFAT) rescues osteoclastogenesis in precursors lacking c-Fos. *J. Biol. Chem.* **279,** 26475–26480
4. Kawaida, R., Ohtsuka, T., Okutsu, J., Takahashi, T., Kadono, Y., Oda, H., Hikita, A., Nakamura, K., Tanaka, S., and Furukawa, H. (2003) Jun dimerization protein 2 (JDP2), a member of the AP-1 family of transcription factor, mediates osteoclast differentiation induced by RANKL. *J. Exp. Med.* **197,** 1029–1035
5. Maruyama, K., Fukasaka, M., Vandenbon, A., Saitoh, T., Kawasaki, T., Kondo, T., Yokoyama, K. K., Kidoya, H., Takakura, N., Standley, D., Takeuchi, O., and Akira, S. (2012) The transcription factor Jdp2 controls bone homeostasis and antibacterial immunity by regulating osteoclast and neutrophil differentiation. *Immunity* **37,** 1024–1036
6. Grigoriadis, A. E., Wang, Z. Q., Cecchini, M. G., Hofstetter, W., Felix, R., Fleisch, H. A., and Wagner, E. F. (1994) c-Fos: a key regulator of osteoclast-macrophage lineage determination and bone remodeling. *Science* **266,** 443–448
7. Franzoso, G., Carlson, L., Xing, L., Poljak, L., Shores, E. W., Brown, K. D., Leonardi, A., Tran, T., Boyce, B. F., and Siebenlist, U. (1997) Requirement for NF-κB in osteoclast and B-cell development. *Genes Dev.* **11,** 3482–3496
8. Glantschnig, H., Fisher, J. E., Wesolowski, G., Rodan, G. A., and Reszka, A. A. (2003) M-CSF, TNFα and RANK ligand promote osteoclast survival by signaling through mTOR/S6 kinase. *Cell Death Differ.* **10,** 1165–1177
9. Tanabe, N., Wheal, B. D., Kwon, J., Chen, H. H., Shugg, R. P., Sims, S. M., Goldberg, H. A., and Dixon, S. J. (2011) Osteopontin signals through calcium and nuclear factor of activated T cells (NFAT) in osteoclasts: a novel RGD-dependent pathway promoting cell survival. *J. Biol. Chem.* **286,** 39871–39881
10. Lee, S. E., Chung, W. J., Kwak, H. B., Chung, C. H., Kwack, K. B., Lee, Z. H., and Kim, H. H. (2001) Tumor necrosis factor-α supports the survival of

osteoclasts through the activation of Akt and ERK. *J. Biol. Chem.* **276,** 49343–49349
11. Xing, L., Venegas, A. M., Chen, A., Garrett-Beal, L., Boyce, B. F., Varmus, H. E., and Schwartzberg, P. L. (2001) Genetic evidence for a role for Src family kinases in TNF family receptor signaling and cell survival. *Genes Dev.* **15,** 241–253
12. Yano, A., Tsutsumi, S., Soga, S., Lee, M. J., Trepel, J., Osada, H., and Neckers, L. (2008) Inhibition of Hsp90 activates osteoclast c-Src signaling and promotes growth of prostate carcinoma cells in bone. *Proc. Natl. Acad. Sci. U.S.A.* **105,** 15541–15546
13. MacLean, M., and Picard, D. (2003) Cdc37 goes beyond Hsp90 and kinases. *Cell Stress Chaperones* **8,** 114–119
14. Takeuchi, O., and Akira, S. (2010) Pattern recognition receptors and inflammation. *Cell* **140,** 805–820
15. Takayanagi, H., Kim, S., Matsuo, K., Suzuki, H., Suzuki, T., Sato, K., Yokochi, T., Oda, H., Nakamura, K., Ida, N., Wagner, E. F., and Taniguchi, T. (2002) RANKL maintains bone homeostasis through c-Fos-dependent induction of interferon-β. *Nature* **416,** 744–749
16. Kawagoe, T., Takeuchi, O., Takabatake, Y., Kato, H., Isaka, Y., Tsujimura, T., and Akira, S. (2009) TANK is a negative regulator of Toll-like receptor signaling and is critical for the prevention of autoimmune nephritis. *Nat. Immunol.* **10,** 965–972
17. Maruyama, K., Kawagoe, T., Kondo, T., Akira, S., and Takeuchi, O. (2012) TRAF family member-associated NF-κB activator (TANK) is a negative regulator of osteoclastogenesis and bone formation. *J. Biol. Chem.* **287,** 29114–29124
18. Fukasaka, M., Ori, D., Kawagoe, T., Uematsu, S., Maruyama, K., Okazaki, T., Kozaki, T., Imamura, T., Tartey, S., Mino, T., Satoh, T., Akira, S., and Takeuchi, O. (2013) Critical role of AZI2 in GM-CSF-induced dendritic cell differentiation. *J. Immunol.* **190,** 5702–5711
19. Inaba, K., Inaba, M., Romani, N., Aya, H., Deguchi, M., Ikehara, S., Muramatsu, S., and Steinman, R. M. (1992) Generation of large numbers of dendritic cells from mouse bone marrow cultures supplemented with granulocyte/macrophage colony-stimulating factor. *J. Exp. Med.* **176,** 1693–1702
20. Trapnell, B. C., Whitsett, J. A., and Nakata, K. (2003) Pulmonary alveolar proteinosis. *N. Engl. J. Med.* **349,** 2527–2539
21. Stanley, E., Lieschke, G. J., Grail, D., Metcalf, D., Hodgson, G., Gall, J. A., Maher, D. W., Cebon, J., Sinickas, V., and Dunn, A. R. (1994) Granulocyte/macrophage colony-stimulating factor-deficient mice show no major perturbation of hematopoiesis but develop a characteristic pulmonary pathology. *Proc. Natl. Acad. Sci. U.S.A.* **91,** 5592–5596
22. Thomassen, M. J., Barna, B. P, Malur, A. G., Bonfield, T. L., Farver, C. F,, Malur, A., Dalrymple, H., Kavuru, M. S., and Febbraio, M. (2007) ABCG1 is deficient in alveolar macrophages of GM-CSF knockout mice and patients with pulmonary alveolar proteinosis. *J. Lipid Res.* **48,** 2762–2768
23. Rosen, S. H., Castleman, B., and Liebow, A. A. (1958) Pulmonary alveolar proteinosis. *N. Engl. J. Med.* **258,** 1123–1142
24. Sato, K., Suematsu, A., Okamoto, K., Yamaguchi, A., Morishita, Y., Kadono, Y., Tanaka, S., Kodama, T., Akira, S., Iwakura, Y., Cua, D. J., and Takayanagi, H. (2006) Th17 functions as an osteoclastogenic helper T cell subset that links T cell activation and bone destruction. *J. Exp. Med.* **203,** 2673–2682
25. Gao, B., Calhoun, K., and Fang, D. (2006) The proinflammatory cytokines IL-1β and TNF-α induce the expression of Synoviolin, an E3 ubiquitin ligase, in mouse synovial fibroblasts via the Erk1/2-ETS1 pathway. *Arthritis Res. Ther.* **8,** R172
26. Zhao, C., Irie, N., Takada, Y., Shimoda, K., Miyamoto, T., Nishiwaki, T., Suda, T., and Matsuo, K. (2006) Bidirectional ephrinB2-EphB4 signaling controls bone homeostasis. *Cell Metab.* **4,** 111–121
27. Maruyama, K., Takada, Y., Ray, N., Kishimoto, Y., Penninger, J. M., Yasuda, H., and Matsuo, K. (2006) Receptor activator of NF-κB ligand and osteoprotegerin regulate proinflammatory cytokine production in mice. *J. Immunol.* **177,** 3799–3805
28. Zhu, H., Guo, Z. K., Jiang, X. X., Li, H., Wang, X. Y., Yao, H. Y., Zhang, Y., and Mao, N. (2010) A protocol for isolation and culture of mesenchymal stem cells from mouse compact bone. *Nat. Protoc.* **5,** 550–560
29. Kuroda, Y., Hisatsune, C., Nakamura, T., Matsuo, K., and Mikoshiba, K. (2008) Osteoblasts induce Ca^{2+} oscillation-independent NFATc1 activation during osteoclastogenesis. *Proc. Natl. Acad. Sci. U.S.A.* **105,** 8643–8648
30. Satoh, T., Takeuchi, O., Vandenbon, A., Yasuda, K., Tanaka, Y., Kumagai, Y., Miyake, T., Matsushita, K., Okazaki, T., Saitoh, T., Honma, K., Matsuyama, T., Yui, K., Tsujimura, T., Standley, D. M., Nakanishi, K., Nakai, K., and Akira, S. (2010) The Jmjd3-*Irf4* axis regulates M2 macrophage polarization and host responses against helminth infection. *Nat. Immunol.* **11,** 936–944